PREPARATIONS FOR REDUCED GRAVITY FLIGHTS TO EXAMINE EXOMARS ROVER WHEEL-SOIL INTERACTIONS

Krzysztof Skonieczny [(1)], Parna Niksirat [(1)], Amir Ali Forough Nassiraei [(1)]

[(1)] Concordia University, 1455 de Maisonneuve Blvd. W., EV-5.139, Montreal, Quebec, Canada, H3G 1M8, kskoniec@encs.concordia.ca

ABSTRACT

Testing in terrestrial gravity can never provide the full picture of planetary wheel-terrain interactions. In preparation for parabolic flights with a prototype ExoMars Rover wheel driving on ES-2 Mars simulant at equivalent Martian gravitational acceleration, automated soil preparation and the structural analysis of the experimental apparatus have turned out to be the most substantial tasks. This work describes how soil preparation can be adapted to the extreme constraints of parabolic flights, and how output port diameter and spacing affect soil loosening performance. It also provides an overview of the planned in-flight experimentation campaign that includes testing of soil preparation quality, extensive wheel-soil interaction experiments, and links of these datasets to telemetry.

1. INTRODUCTION

The Global Exploration Roadmap, to which the Canadian Space Agency (CSA) and European Space Agency (ESA) are signatory, identifies Mars, the Moon, and asteroids as priority destinations [1]. The terrains of Mars and the Moon consist of fine granular regolith with embedded rocks, as do those of a recently discovered class of "rubble-pile" asteroids [2, 3]. Understanding the nature of interactions with granular terrains is thus crucial to exploring these high priority destinations. The entrapment of the Mars Exploration Rover Spirit in soft regolith and the tears and punctures in the Mars Science Laboratory Curiosity rover's wheels demonstrate some of the current mobility challenges of such granular terrains. In particular, understanding such challenges would be very beneficial to ESA's ExoMars rover mission.

This research studies robot mobility in granular terrains, specifically the effects of reduced gravity on wheel-soil interactions.

Classical wheel-terrain interaction models used in the literature are unable to sufficiently predict the effects of reduced gravity on rover performance. The founding modeling paradigm of terramechanics (the study of vehicle-terrain interactions) relies on quasi-static pressure sinkage relationships to estimate compaction resistance [4] and/or empirical parameters, e.g. to estimate the location of maximum pressure beneath a wheel [5]. For rigid wheels on dry granular soil – a typical case for planetary rovers – the quasi-static assumption is contradicted by the data; Wong observed flowing granular soil, and pressure distributions more complex than predicted by quasi-static compaction [6]. In Section 1.1.3, we present recent work that adds further evidence and details of this complex granular flow.

Empirical parameters in terramechanics models can pose difficulties when extrapolating to new conditions, such as extraterrestrial regolith and gravity. For example, to account for results of recent wheel traction experiments in reduced-g flights by Kobayashi [7] within the pressure-sinkage paradigm, a pressure-sinkage coefficient proportional to g has been hypothesized by Wong [8]. However, pressure-sinkage coefficients can be directly extracted from data of yet another set of reduced-g flight experiments by Bui, and are in fact constant across measurements at 1 g, 1/2 g, or 1/6 g [9]. This inability to reconcile classical terramechanics theory with all available experimental data suggests a need to rethink model assumptions and develop new models for planetary rover-soil interactions.

Several researchers today highlight the insufficient predictive power of classical terramechanics models for planetary rovers [10-13]. They have proposed modifying or adding model parameters; insufficiency of the base model assumptions has yet to be addressed.

There is existing literature describing wheel-soil interaction experiments during reduced gravity flights, as alluded to above. Only a single dataset has been collected for wheels driving in soil during reduced-g flights: the work of Kobayashi [7]. This dataset is based on a self-propelled wheel driving in FJS-1 lunar soil simulant and in Toyoura sand in a wide range of gravity conditions: 1/6 g, 1/2 g, 3/4 g, 1 g, and 2 g. However, the actual data collected is limited; it includes just horizontal travel distance, vertical sinkage, and wheel torque. The data is contrasted to a dataset collected in 1 g that is corresponding but with varying vertical load on the wheel (i.e. 1/6 W, 1/2 W, etc.). The difference between the experimental conditions in the two datasets is the effect of gravity on the soil particles themselves. Kobayashi's key observation is that wheel travel is

impaired when both the wheel and soil are in reduced gravity, rather than improving as it does when just the load on the wheel is reduced [7]. Another observation, that may in fact explain the first, is that wheel sinkage is not affected significantly by the gravity conditions. This research intends to directly study these prior observed phenomena along the way to advancing the state of scientific knowledge with new test conditions and greatly enhanced datasets.

In Kobayashi's experiments, as well as in similar terramechanics experiments in reduced-g flights of excavation [14] and bearing capacity [9], the effects of soil preparation are not explored directly but rather taken for granted to be negligible. Experimentation to test this assumption is also previewed here.

2. PLANNED EXPERIMENTATION

We are currently preparing for an experimentation campaign in Fall 2017 that will characterize wheel-soil interactions in reduced gravity. Martian and lunar g will be achieved in parabolic flight. Wheel slip and normal load will be controlled, and sinkage, wheel current (to estimate wheel torque), forces and torques, and soil flow will all be measured.

2.1. Reduced-g Flight Campaign

With technical support and funding from the CSA, we will be conducting a series of parabolic flights aboard Canada's National Research Council's (NRC) Falcon 20 aircraft.

The flights will subject the experiments to reduced-g at Martian (3.7 m/s^2) and lunar (1.62 m/s^2) levels. Martian gravity is studied to provide direct mission relevance to ExoMars. Lunar gravity is studied because it at the extreme end of low gravity considered relevant for wheeled rovers, and thus is useful for investigating general trends in reduced g. The campaign will include 30 parabolas, with 15 at each gravitational acceleration.

The 30 parabolas include 24 for studying wheel-soil interactions and 6 for studying in-flight soil preparation; both these types of experiments are described in subsequent subsections.

2.2. Wheel-Soil Interaction Experiments

The main experimental apparatus consists of a sandbox beneath a robotic gantry that drives a wheel through the soil in the box. The gantry consists of a linear actuator that advances the wheel, a motor that turns the wheel, pneumatic actuators that apply a downward force on the wheel. By these mechanisms the wheel's slip rate and normal force are controlled. The designed apparatus is shown in Fig. 1.

Through an in-kind contribution agreement with MDA, the wheel that will be tested during the reduced-g flight campaign is a prototype ExoMars Rover wheel.

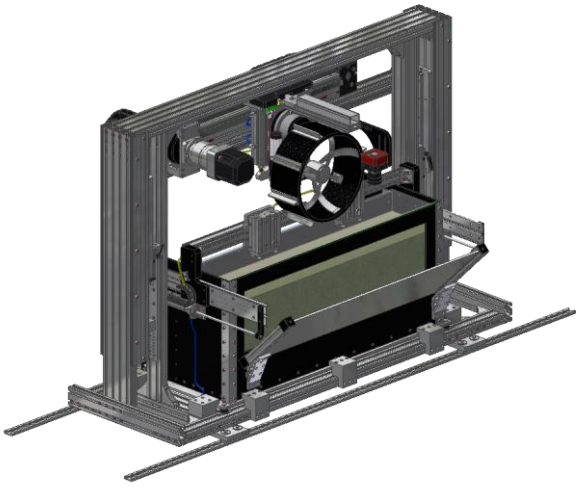

Figure 1. Wheel-soil interaction experiment testbed for reduced-g flights, mounted to aircraft seat rails. The apparatus consists of a sandbox and robotic gantry with wheel assembly (basic example wheel shown).

The experimental apparatus measures wheel traction forces using a 6-axis Force-Torque sensor (ATI Delta IP65), sinkage using a linear potentiometer, and motor current (Maxon RE35) to estimate wheel torque. In addition, we have developed an experimental technique for visualizing and analyzing robotic interactions with granular terrain, the Soil Optical Flow Technique (SOFT). It uses the computer vision techniques of optical flow and clustering to process images of soil interacting with a wheel from high-speed photos (IO Flare 4M180-CL with 16mm EFL, f/1.4 lens) taken through a glass wall of a soil bin. The richness of the data produced, see Fig. 2, highlights gaps and discrepancies in existing terramechanics models and enables validation of new models that approach robot-terrain interactions with an appropriate and efficient level of detail.

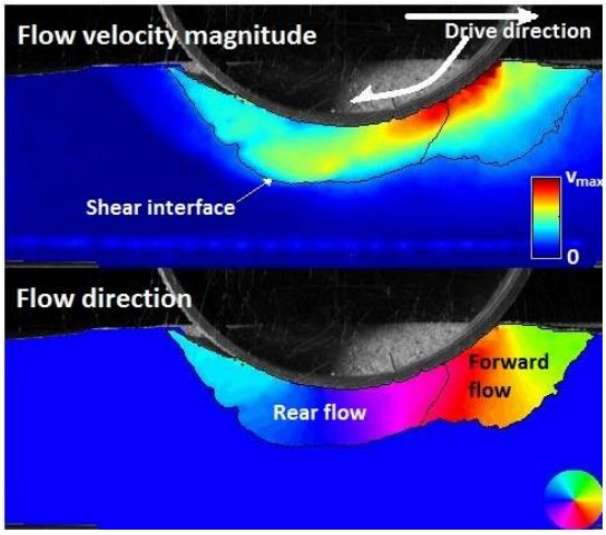

Figure 2. The Soil Optical Flow Technique (SOFT) visualizes soil flow as it interacts with a wheel during experiments.

2.3. Soil Preparation Experiments

Flight operational constraints impose short 15-20 s periods of reduced gravity separated by only a further 60 s or so. These time constraints motivate automated operation, data collection, and soil preparation. Periods of reduced-g are immediately preceded by periods of high-g (~2g). One of the research objectives of this work is to investigate the effects of this prior high-g loading on soil parameters during subsequent reduced-g.

Soil preparation for terramechanics experimentation consists of loosening, compacting, and leveling soil to achieve repeatable soil parameters. In previous research, we conducted such preparation manually [15]. Due to time constraints aboard reduced gravity flights, these tasks will be automated. During soil preparation, the test implement will be removed from the soil bin, which will then be covered with a flat pressing plate that fits within its walls. Loosening will involve shooting jets of compressed air through the soil via flexible one-way nozzles at the base of the bin. The loosening method is the subject of the subsequent section.

Compaction and leveling will be achieved together by vibrating the bin and lowering the pressing plate at a controlled pressure to a desired depth (and thus bulk density). Air jets and vibration under pressure are rapid techniques for loosening and compacting soil, respectively.

The quality of the soil preparation achieved will be validated by measuring the resulting soil properties using a high quality cone potentiometer (Rimik CP40ii). Consistency of soil preparation between different areas of the testbed, and between subsequent runs of the equipment, will be analyzed statistically.

The objective of this experiment is to identify whether there is a significant difference in resulting soil properties depending on when soil preparation occurs within the phases of a reduced-g flight. This experiment will require 6 parabolas at lunar g, selected to provide the largest contrast to 1-g among gravity levels relevant to wheeled rovers.

Automated soil preparation will be executed during the period of lunar g for 3 of the flights, and during the period of 1 g for the remaining 3. Soil properties will then be measured with a cone penetrometer during the period of lunar gravity in both cases. The repetition of each condition in triplicate will enable subsequent statistical analysis.

3. SOIL LOOSENING EXPERIMENTS

A crucial function of the automated soil preparation subsystem is soil loosening. The ability to achieve evenly distributed loosening using jets of air was unknown, so a research program was undertaken to addresses this technical risk.

The loosening should be achieved across the entire area of soil, and also through as much of the depth as possible. The lateral sand displacement profile and the depth at which motion boundaries are observed are thus both studied.

Pneumatic manifolds are used to distribute air flow to multiple outputs through which the jets or air are shot. Some of the key design variables for a manifold are its inner diameter (D), the number (N_i) and diameter (D_i) of input inlets, the number (N_o) and diameter (D_o) of output ports, and the distance between open output ports (called the pitch), and the inlet pressure. The diagram in Fig. 3 indicates these key features.

It is desired to achieve even loosening for soil prepared to a height of at least 30 cm. Two soil types are studied: beach sand and ES-2 Martian simulant [16].

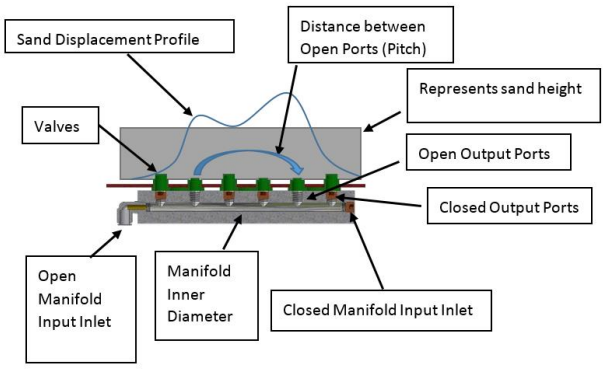

Figure 3. Key design variables and performance indicators for an air distribution manifold.

Many factors affect the velocity, airflow and pressure drop in a manifold, as can be explained through a theoretical analysis of such flow [17]. Wang identifies the structure parameter M (ratio of sum of all the output port areas to cross-sectional area of the pipe inside the manifold, i.e. $N_oD_o^2/D^2$) on axial velocity, flow distribution and pressure drop along the manifold. M affects the airflow distribution across the manifold output ports. For smaller values of M, the airflow is more uniform and consistent.

Also the influence of the structure parameter E (Ratio of manifold length to diameter (L/D)) on the flow distribution and the pressure drop in the ports has been presented by Wang. In this equation length is considered to be the distance from the first open port to the last open output port of the manifold. Again, the smaller the value of E, the more uniform the flow distribution. To adjust the value of E it is required to either change the diameter of the manifold (which means replacing the manifold) or to change the distance between open ports, i.e. pitch, to modify L.

A very broad simplification is thus that smaller output ports, smaller D_o, produce more uniform air flow (smaller M). It is also easier to achieve uniform flow with fewer output ports, i.e. smaller N_o (again, smaller M, assuming fixed D_o). On the other hand, with a fixed N_o, closer spacing, smaller pitch, improves uniformity (smaller E). As points of reference, Wang explores values of M between 0.5 and 3, and values of E between 3 and 100 [17].

Of course, the uniformity of the flow must be traded off against the scale of the distribution of the flow. A small number of closely spaced output ports may not be capable of loosening a large area of soil. Each output port has an effective area of influence, and these must overlap to achieve loosening of the entire area.

Furthermore, the uniformity of the air flow does not take into account its effectiveness in actually displacing sand. Very low values of M mean the output port diameters are very small. For incompressible flow, this corresponds to high velocity and low pressure. However, there is a minimum outlet pressure required to displace soil of a given height and, correspondingly, mass.

3.1. Output Port Diameter and M

A set of initial experiments was conducted to study the effects of increasing output port diameter, and thus M, on sand loosening performance. A 6 port manifold was mounted beneath a box containing beach sand. Soft plastic valves were placed between open output ports and the box to prevent soil entering the manifold. The manifold had an inner diameter, D, of 5 mm. Experiments were conducted using ports 2 and 5, at a pitch of 90 mm (E = 18). The inlet pressure was set to 95 psi.

As the two circular output port diameters were increased from 2 mm (M = 0.125) through 3.1 mm and 4.3 mm to 5 mm (M = 2), the height of sand successfully displaced continually improved from less than 8 cm to over 16 cm, respectively. Furthermore, the soil loosening that was achieved was visibly uniform across the length of the sandbox.

With two output ports of diameter 8 mm (M = 5), however, the soil loosening was no longer uniform.

An important lesson learned from this set of experiments concerned the effect of output hole geometry on flow properties. To alter the diameter of the output port of the manifold, holes were drilled into inserts and screwed into the output ports (an open output port with no insert had an 8mm diameter). Each insert had a 6mm hex socket for screwing it into place. A 5mm hole approaches the edges of the 6mm hex socket. Initially, 5 mm output holes prepared in this fashion demonstrated a sudden drop off in performance. Further research has provided insight into the characteristics of turbulent flow due to the hexagon orifice that effects the outline of the flow, as described by Wang et al. [18]. Because the hole was too close to the inside contour of the hex socket the flow suffered from a special phenomenon referred to as hexagon orifice flow. To avoid this effect, 5 mm output port diameters were instead achieved by inserting a smooth plastic pipe of 5 mm inner diameter and 8 mm outer diameter into the standard output ports.

Note that diameters between 5 mm and 8 mm were not explored for practical reasons, as we did not have other pipes available and if such holes were drilled into the inserts it would render them unusable. From the results of these experiments, however, it is possible to conclude that values of M less than or equal to 2 produce sufficiently uniform flow.

3.2. Output Port Pitch and Soil Height

In order to improve sand displacement performance further, other aspects of the system (aside from output port diameter) were modified. The inner diameter of the manifold has been upgraded from 5mm to 8mm, making it easier to keep flow distribution uniform by reducing both M and E. The input valve to the manifold (the connection between the manifold and the compressor), which previously was the bottleneck of the system, has also been increased in diameter (from 5 to 18mm), as has the pipe connecting the compressor to the manifold. The length (i.e. maximum pitch) of the manifold is increased from 150 to 300mm, which provides a

possibility to experiment with greater distances between the open output ports. This next phase of the experimentation keeps M in the desired range, below 2; in fact it is no greater than 0.8.

The above-mentioned modifications immediately enabled the system to achieve uniform soil loosening of beach sand of a height of 25 cm, with D_o = 5 mm and a pitch of 90 mm.

With a sand height of 25 cm, the pitch was then increased until a noticeable performance drop was observed. At a pitch of 210 mm, uniform soil displacement was still observed. The same experiment with the pitch of 240, resulted in an uneven sand displacement at the center due to receiving less airflow from the open output ports which were farther away from the center. This same result of satisfactory loosening at a pitch of 210 mm, but unsatisfactory loosening at a pitch of 240 mm, was observed with output port diameters, D_o, of 5 mm, 4 mm, and 3 mm. Furthermore, these results were robust to a pressure drop from the nominal 95 psi to 60 psi for D_o of 4 mm or 5 mm; on the other hand, they were very sensitive to the pressure drop for D_o = 3 mm.

The experiments at a pitch of 240 mm discussed above (with Do = {3 mm, 4 mm, 5mm} and p = 95 psi) were repeated with the height of the sand increased to 31cm. It was interesting to observe that after increasing the height of the sand, the sand displacement at the center actually improved. In comparison to the 25 cm height experiments, where the regions of the sand at the center didn't move, increasing the height of the sand resulted into a more uniform displacement across all regions. This could perhaps be due to the pressure exerted from the weight of the extra sand which resulted the airflow to diverge and cover the mid-section.

Increased sand height also made the results much more sensitive to pressure drops, though. For sand of 31 cm height, at a pitch of 240 mm and p = 60 psi, no displacement was achieved with any of the three output port diameters.

Additional experiments were conducted with just a single output port open, to observe the profile of the displaced sand. Note that these results are not directly comparable to those with multiple open ports as the outlet pressure is affected by the number of outlets. Although the sand displacement is visible in the videos of the experiments, it is difficult to capture in a screenshot. For this reason, schematic diagrams of the results are presented in Fig. 4. Sand displacement occurs in a narrow region near the bottom of the sandbox, and then spreads out. The degree of this subsequent spreading, as well as the depth at which the transition occurs, depends on the inlet pressure (and also soil type and other factors, as will be seen in the next section).

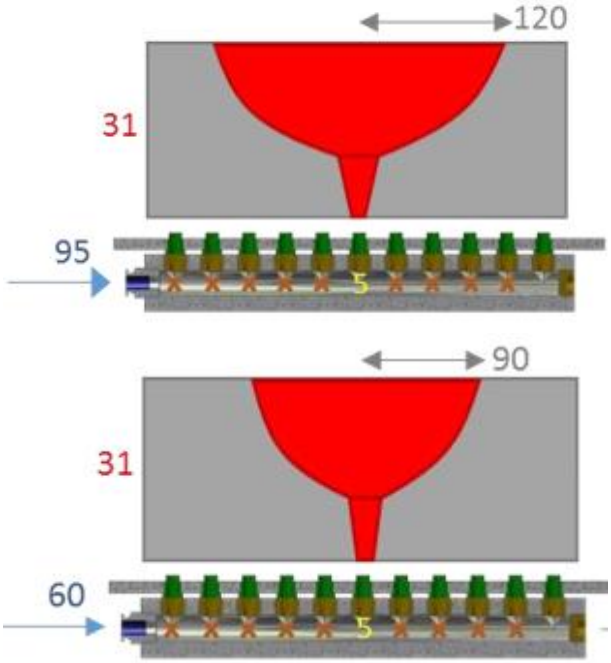

Figure 4. Single output port experiments show that the effective loosening area spreads to a radius of 120 mm at 95 psi, and 90 mm at 60 psi.

3.3. Depth of Motion Boundary and ES-2

As discussed earlier, the depth at which motion boundaries are observed in the soil provides an indication of how evenly the soil is loosened throughout its depth.

ES-2 Mars simulant is a soil of great relevance to the ExoMars Rover mission, as it represents an analogue for fine Aeolian sand that has proven challenging for the MER and Curiosity rovers. ES-2 is also a soil that is particularly well suited for observing soil motion boundaries.

Repeating one of the successful configurations from earlier experiments with beach sand (D_o = 4 mm, pitch = 240 mm, p = 95 psi, height = 31 cm), it could be observed that with ES-2 the depth of the soil motion boundary was quite shallow at approximately 5 cm. This is depicted schematically in Fig. 5, with video screenshots shown in Fig. 6.

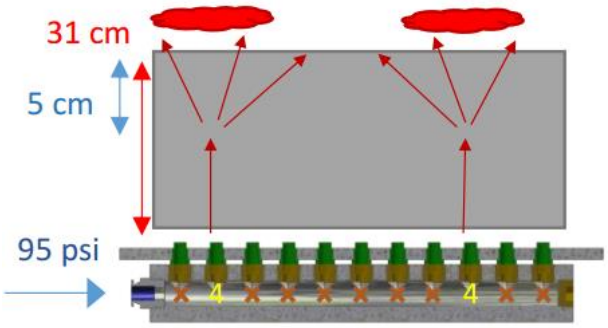

Figure 5. Experiments with D_o = 4 mm and pitch = 240 mm (M = 0.5, E = 30) in ES-2 result is a shallow motion boundary.

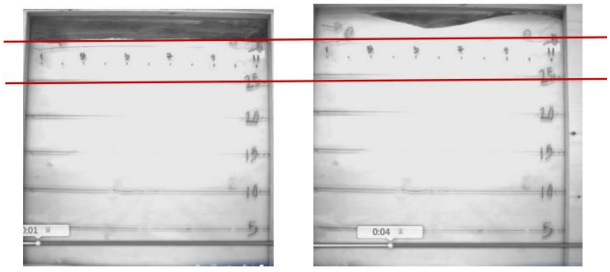

Figure 6. Screenshots before (left) and during (right) air flow with a shallow soil motion boundary. M = 0.5, E = 30.

To improve the soil loosening throughout the depth of the soil, an increase in the output port diameter was attempted. For an initial comparison, the screw inserts were simply removed leaving 20 mm diameter openings (for the larger manifold in the new setup introduced first in Section 3.2). As this results in a dramatic increase of M from 0.5 to 12.5, the pitch between open output ports was reduced to counter some of the non-uniformity in the flow (reducing E from 30 to 15). With this new configuration, soil loosening was achieved throughout almost the entire depth of the soil, as shown in Fig. 7 and Fig. 8.

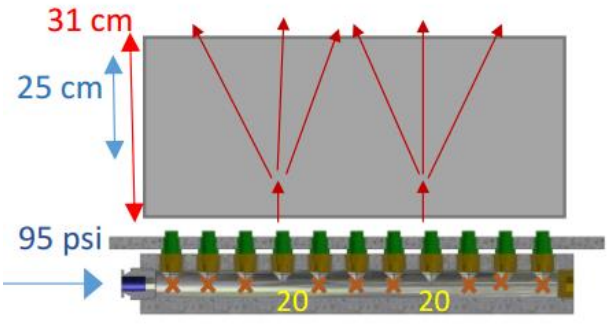

Figure 7. Experiments with Do = 20 mm and pitch = 120 mm (M = 12.5, E = 15) in ES-2 result is a deep motion boundary.

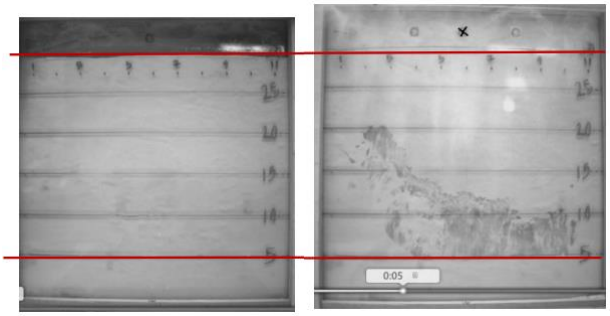

Figure 8. Screenshots before (left) and during (right) air flow with a deep soil motion boundary. Note the voids visible in the bottom half of the right image. M = 12.5, E = 15.

Further tests will continue investigating configurations with smaller and farther-spaced output ports.

4. STRUCTURAL ANALYSIS

The structural modelling and analysis of the experimental apparatus has been one of the most significant tasks in preparation for the parabolic flight campaign. A simplified but fully representative model of the apparatus was prepared in Femap (see, for example, Fig. 9).

Load analyses were conducted with Femap's NASTRAN engine for emergency flight conditions including 9 g accelerations in the aft direction in case of emergency landing. Forces and moments at fastener junctions were evaluated to ensure there are no failures causing the apparatus to break apart or to break free from the seat rails.

The sandbox was also analysed to determine that it can withstand the same emergency load cases, during which the soil will induce hydrostatic-like forces on the aluminium and tempered-glass walls of the sandbox, as shown in Fig. 10.

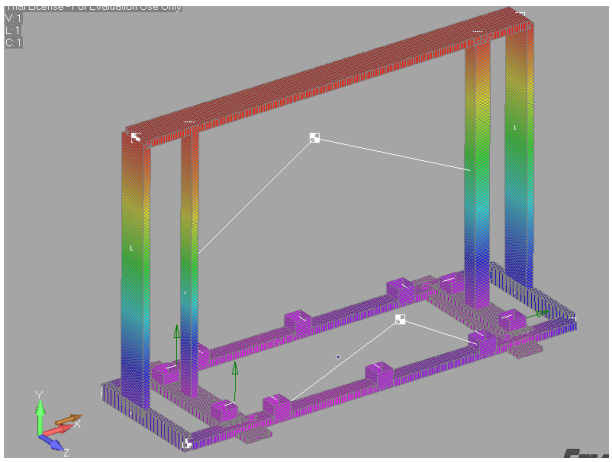

Figure 9. Representative structural model of the in-flight experimental apparatus (compare to Fig. 1).

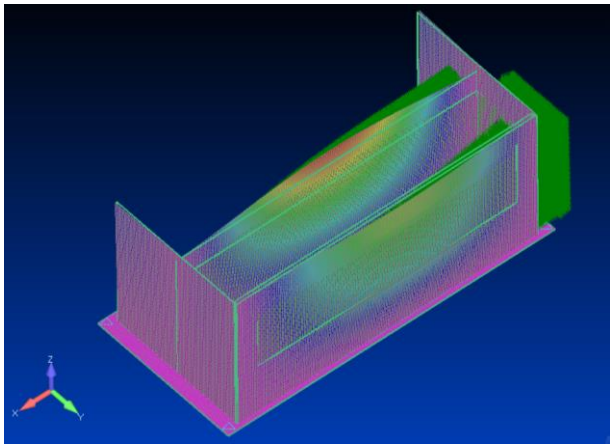

Figure 10. Structural analysis of the sandbox considering hydrostatic-like soil loads from 9 g emergency loads in the aft (-x here) direction.

5. CONCLUSIONS AND FUTURE WORK

In preparation for parabolic flights with a prototype ExoMars Rover wheel driving on ES-2 Mars simulant at equivalent Martian gravitational acceleration, the development of an automated soil preparation subsystem and the structural analysis of the experimental apparatus have turned out to be the most substantial tasks.

For automated soil loosening using jets of air, it is important to have sufficiently large output port diameters in the manifold that distributes air throughout the sandbox. For beach sand, output ports of at least 4 mm are recommended; smaller diameter outputs are sensitive to pressure drops. For ES-2 Mars simulant, larger output diameters are recommended (20 mm tested) to achieve soil loosening throughout the entire depth of the soil.

To achieve uniformly distributed soil loosening, output port diameter and spacing should be balanced in a way to try to keep the parameters M (ratio of sum of all the output port areas to cross-sectional area of the pipe inside the manifold) and E (ratio of manifold length to diameter (L/D) low. Consistent results have been achieved with $M < 2$ and $E < 20$.

Another lesson learned for soil loosening is to ensure that output ports are kept circular to avoid hexagonal orifice flow (possible if hole diameters approach the edges of a hex socket used to screw in output port inserts).

An interesting observation is that soil loosening distribution can sometimes be improved by adding soil height. In comparing experiments with 31 cm of sand to those with 25 cm height, where the regions of the sand at the center didn't move, increasing the height of the sand resulted into a more uniform displacement across all regions. This could perhaps be due to the pressure exerted from the weight of the extra sand which resulted the airflow to diverge and cover the mid-section.

The experiments described in this work will fly aboard Canada's National Research Council's (NRC) Falcon 20 aircraft in Fall 2017.

The ExoMars wheel-soil interaction dataset created in reduced-g will also link telemetry-like data (motor current, slip, etc.) to the extensive experimental dataset (visualized wheel-soil interactions, sinkage) to provide a powerful contextual tool for future operators to ultimately interpret rover telemetry.

6. REFERENCES

1. 1. Int. Space Exploration Coordination Group (ISECG). (2013). The global exploration roadmap.
2. Fujiwara, A., Kawaguchi, J., Yeomans, D. K., Abe, M., Mukai, T., Okada, T. & Uesugi, K. (2006). The rubble-pile asteroid Itokawa as observed by Hayabusa. *Science*, *312*(5778), 1330-1334.
3. Rozitis, B., MacLennan, E., & Emery, J. P. (2014). Cohesive forces prevent the rotational breakup of rubble-pile asteroid (29075) 1950 DA. *Nature*, *512*(7513), 174-176.
4. Bekker, M. G. (1956). Theory of land locomotion. University of Michigan.
5. Wong, J. Y., & Reece, A. R. (1967). Prediction of rigid wheel performance based on the analysis of soil-wheel stresses part I. Performance of driven rigid wheels. *Journal of Terramechanics*, *4*(1), 81-98.
6. Wong, J. Y. (1967). Behaviour of soil beneath rigid wheels. *Journal of Agricultural Engineering Research*, *12*(4), 257-269.
7. Kobayashi, T., Fujiwara, Y., Yamakawa, J., Yasufuku, N., & Omine, K. (2010). Mobility performance of a rigid wheel in low gravity environments. *Journal of Terramechanics*, *47*(4), 261274.
8. Wong, J. Y. (2012). Predicting the performances of rigid rover wheels on extraterrestrial surfaces based on test results obtained on earth. *Journal of Terramechanics*, *49*(1), 49-61.
9. Bui, H. H., Kobayashi, T., Fukagawa, R., & Wells, J. C. (2009). Numerical and experimental studies of gravity effect on the mechanism of lunar excavations. *Journal of terramechanics*, *46*(3), 115-124.

10. Meirion-Griffith, G., & Spenko, M. (2011). A modified pressure–sinkage model for small, rigid wheels on deformable terrains. *Journal of Terramechanics*, *48*(2), 149-155.
11. Ding, L., Deng, Z., Gao, H., Tao, J., Iagnemma, K. D., & Liu, G. (2014). Interaction Mechanics Model for Rigid Driving Wheels of Planetary Rovers Moving on Sandy Terrain with Consideration of Multiple Physical Effects. *Journal of Field Robotics*. In press.
12. Irani, RA et al (2011). A dynamic terramechanic model … *J Terramechanics*, *48*(4), 307-318.
13. Senatore, C., & Iagnemma, K. (2014). Analysis of stress distributions under lightweight wheeled vehicles. *Journal of Terramechanics*, *51*, 1-17.
14. Boles, W. W., Scott, W. D., & Connolly, J. F. (1997). Excavation forces in reduced gravity environment. *Journal of Aerospace Engineering*, *10*(2), 99-103.
15. Skonieczny, K., Moreland, S. J., Asnani, V. M., Creager, C. M., Inotsume, H., & Wettergreen, D. S. (2014). Visualizing and Analyzing Machine_soil Interactions using Computer Vision. *Journal of Field Robotics*, *31*(5), 820-836.
16. Gouache, T. P., Patel, N., Brunskill, C., Scott, G. P., Saaj, C. M., Matthews, M., & Cui, L. (2011). Soil simulant sourcing for the ExoMars rover testbed. *Planetary and Space Science*, *59*(8), 779-787.
17. Wang, J. (2011). Theory of flow distribution in manifolds. *Chemical engineering journal*, *168*(3), 1331-1345.
18. Wang, W., Nicolleau, F. C., & Qin, N. (2016). Comparison of turbulent flow through hexagram and hexagon orifices in circular pipes using large-eddy simulation. *Fluid Dynamics Research*, *48*(2), 021408.